Journal of Applied Physics

RESEARCH ARTICLE | JULY 23 2025

Atomic order induced reduction of Gilbert damping constant and enhancement of half-metallicity in off-stoichiometric $Co_2FeGa_{0.5}Ge_{0.5}$ Heusler alloy thin films

Madhav M. Bhat ; K. Simalaotao ; H. Suto ; A. Perumal ; A. Srinivasan ; Y. Sakuraba

J. Appl. Phys. 138, 043904 (2025)
https://doi.org/10.1063/5.0268776

Journal of Applied Physics ARTICLE pubs.aip.org/aip/jap

Atomic order induced reduction of Gilbert damping constant and enhancement of half-metallicity in off-stoichiometric $Co_2FeGa_{0.5}Ge_{0.5}$ Heusler alloy thin films

Cite as: J. Appl. Phys. **138**, 043904 (2025); doi: 10.1063/5.0268776
Submitted: 4 March 2025 · Accepted: 1 July 2025 ·
Published Online: 23 July 2025

View Online Export Citation CrossMark

Madhav M. Bhat,[1,2] K. Simalaotao,[2,3] H. Suto,[2,a)] A. Perumal,[1] A. Srinivasan,[1,b)] and Y. Sakuraba[1,2,3]

AFFILIATIONS

[1]Department of Physics, Indian Institute of Technology Guwahati, Guwahati 781039, India
[2]Research Center for Magnetic and Spintronic Materials, NIMS, Tsukuba 305-0047, Japan
[3]Graduate School of Pure and Applied Sciences, University of Tsukuba, Tsukuba 305-8571, Japan

[a)]**Author to whom correspondence should be addressed:** SUTO.Hirofumi@nims.go.jp
[b)]**E-mail:** asrini@iitg.ac.in

ABSTRACT

The development of energy-efficient spintronic devices with enhanced magnetoresistance demands materials with low Gilbert damping constant (α) and high half-metallicity. In this study, we report a very low α in sputter-deposited off-stoichiometric $Co_2FeGa_{0.5}Ge_{0.5}$ (CFGG) Heusler alloy thin films and investigate the relation between α and atomic ordering and half-metallicity. CFGG thin films with a composition of $Co_{44.3}Fe_{30.7}Ga_{13.9}Ge_{11.1}$ were epitaxially deposited on MgO (001) substrates by magnetron sputtering followed by *in situ* annealing. The density of states calculations revealed that this composition has higher half-metallicity than the stoichiometric composition, owing to Fermi energy tuning. As-deposited and 400 °C-annealed samples exhibited *B*2-type partially disordered structure, while annealing above 500 °C induced a $L2_1$-type ordered structure. The improvement in atomic order resulted in the reduction of α, as demonstrated by ferromagnetic resonance measurement, and enhancement in half-metallicity, as revealed by anisotropic and ordinary magnetoresistance measurements. The 600 °C-annealed samples exhibited an intrinsic α of $(3.5 \pm 0.3) \times 10^{-4}$, the low value reported for metallic ferromagnetic materials, demonstrating the potential for its use in energy-efficient spintronic devices.

I. INTRODUCTION

The development of energy-efficient spintronic devices demands materials with low Gilbert damping constant (α), because the critical current density for device operation is directly related to α of the active layer material.[1] Extensive studies have been conducted to realize low α materials, and CoFe is one of the conventional magnetic materials with low α with reported α_{int} of $(5.0 \pm 1.8) \times 10^{-4}$ and α_{total} of $(2.1 \pm 0.1) \times 10^{-3}$.[2] Note that the experimentally measured α_{total} is a sum of intrinsic (α_{int}) and extrinsic (α_{ext}) contributions, where the former represents the material parameter and the latter represents the effect of the measurement setup. As different approaches, doping and interfacial modification have been reported to affect α.[3–8] Half-metallic Heusler alloys, which have a novel electronic structure with electron of only one type of spin at the Fermi energy level (E_F), are promising low α materials. Because α_{int} is considered to be proportional to the density of states (DOS) at E_F,[9–11] the presence of only one type of electronic spin (either up or down) DOS at E_F in half-metallic material can result in small DOS at E_F leading to low α. Furthermore, the part of spin scattering channels, such as spin-flip scattering, is forbidden due to half-metallicity, leading to a further reduction in damping. There have been several attempts to minimize α in Heusler alloys by enhancing the half-metallicity,[12,13] and reported α_{total} values ranging from 4.1×10^{-4} to 7.0×10^{-4},[14,15] which are lower than those of 3*d* transition magnetic materials.

Half-metallicity is also advantageous for obtaining large magnetoresistance (MR) output and high spin-transfer torque (STT) efficiency of the devices,[16] and studies on these properties have been extensively carried out on various Heusler alloys. Among them, Co_2Fe based $Co_2FeGa_{0.5}Ge_{0.5}$ (CFGG) has gathered considerable attention with the demonstration of enhanced MR ratio in the current-perpendicular-to-plane giant magnetoresistance (CPP-GMR) device[17–19] due to high spin polarization (P) and a Curie temperature (T_C) of 1080 K.[20] Similarly, Co_2Mn based Heusler alloys are known for high P and have demonstrated significant MR ratios in CPP-GMR devices.[21–25] However, the finite solubility of Mn in Ag spacer reduces the MR.[26,27] These findings have focused research interest on CFGG. Goto *et al.*[28] have shown that the stoichiometric CFGG alloy has Co–Fe disorder arising from Co atoms occupying Fe sites. This disorder introduces minority DOS in the half-metallic gap, thereby decreasing the half-metallicity. Chen *et al.*[29] have conducted a comprehensive study on the effect of CFGG composition on phase stability and half-metallicity and noted that $Co_{39.4}Fe_{29.3}Ga_{13.4}Ge_{17.9}$ exhibits a single-phase with $L2_1$-type structure and increased half-metallicity due to reduced Co–Fe disorder. Based on these findings, α is expected to be reduced by using Co-deficient and Fe-rich off-stoichiometric composition as α is closely related to half-metallicity. However, only the bulk α value (~0.008) is available in the literature,[20] and thus detailed studies on α of CFGG thin films have been demanded.

In this study, we report a very low α in CFGG thin films, focusing on Co-deficient and Fe-rich off-stoichiometric composition, and investigate the relation of α of the film with atomic ordering and half-metallicity. Epitaxial off-stoichiometric CFGG thin films deposited under ambient conditions were annealed at different temperatures (T_{an}) to induce various degrees of atomic ordering, which were examined by x-ray diffraction (XRD). The change in the half-metallicity was assessed by anisotropic magnetoresistance (AMR) and ordinary magnetoresistance (OMR) measurements. An increase in the magnitude of the negative AMR ratio and an increase in the OMR ratio with an increase in T_{an} indicate an enhancement in half-metallicity of the films due to improvement in atomic ordering. The α_{int} of CFGG determined by ferromagnetic resonance measurement decreased with increasing T_{an}, achieving a very low α_{int} of $(3.5 \pm 0.3) \times 10^{-4}$ at $T_{an} = 600$ °C. These results illustrate the relation between α_{int} and half-metallicity and demonstrate the potential of off-stoichiometric CFGG as a low α and high spin polarization material.

II. EXPERIMENTAL AND CALCULATION METHODS

Off-stoichiometric CFGG epitaxial thin films were deposited on single-crystal MgO (001) substrates using a high (>99.9%) purity alloy target of composition $Co_{46.5}Fe_{24.1}Ga_{13.7}Ge_{15.7}$. The deposition was carried out at room temperature using an ultrahigh vacuum radio frequency magnetron sputtering system (Eiko ES-350) with a deposition rate of ~1.2 nm/min. Prior to deposition, the sputtering chamber was evacuated to a base pressure of $\sim 10^{-7}$ Pa. High-purity (~99.999%) argon gas at a pressure of $\sim 4 \times 10^{-1}$ Pa was used as the sputtering gas. During the deposition, a target-to-substrate distance of 100 mm was maintained. The as-deposited thin films were then annealed *in situ* in the vacuum chamber at 400, 500, and 600 °C for 30 min each to improve the atomic ordering. A 2 nm aluminum capping layer was deposited on the annealed films after cooling down. All the CFGG thin films were deposited under the same sputtering condition, and the composition estimated by x-ray fluorescence spectroscopy was in the range of $Co_{44.3\pm0.7}Fe_{30.7\pm1.2}Ga_{13.9\pm0.3}Ge_{11.1\pm0.2}$, indicating the small composition difference among the samples. The atomic order was determined from XRD patterns recorded with Rigaku Smartlab equipped with Cu-$K\alpha$ radiation ($\lambda = 1.5406$ Å) in parallel beam geometry. Using x-ray reflectivity measurement, the thickness and roughness of the samples were found to be ~24 ± 1 and ~0.7 nm, respectively. For quantitative analysis of half-metallicity in the samples, temperature dependent AMR and OMR measurements were carried out using the DC four-probe method in the temperature range of 10–300 K with a physical property measurement system (PPMS, Quantum Design USA). During AMR measurement, 0.2 mA direct current was passed along the ⟨110⟩ direction of the sample, while changing the saturation magnetization direction within the sample plane over 360° by applying a magnetic field of 1 T. The AMR ratio was evaluated by $\Delta\rho/\rho_0$, with $\Delta\rho = \rho_\varphi - \rho_\perp$. Here, ρ_φ and $\rho_\perp$ are the electrical resistivity at an angle φ and 90° between the magnetization and the current direction, respectively. During the OMR measurement, 0.1 mA direct current was passed along the ⟨110⟩ direction of the sample, while varying the magnetic field from 0 to 14 T oriented in a sample plane and perpendicular to the current direction. OMR ratio was evaluated by $\Delta\rho/\rho_0$, with $\Delta\rho = \rho_H - \rho_0$, where ρ_H and ρ_0 are the electrical resistivity in the presence and absence of magnetic field, respectively. The Gilbert damping parameter α was evaluated from in-plane ferromagnetic resonance (FMR) measurements in the frequency range from 16 to 36 GHz using a Phase FMR-40 broadband FMR setup connected to the PPMS. The obtained FMR spectra were fitted to the equation,[30]

$$\frac{dI}{dH} = A_1 \frac{\left[(\Delta H/2)^2 - (H - H_r)^2\right]}{\left[(\Delta H/2)^2 + (H - H_r)^2\right]^2} + A_2 \frac{2(H - H_r)(\Delta H/2)}{\left[(\Delta H/2)^2 + (H - H_r)^2\right]^2}. \quad (1)$$

This fitting allowed for the extraction of the resonance field ($\mu_0 H_r$) and linewidth ($\mu_0 \Delta H$), which were used to calculate α. In Eq. (1), dI/dH represents the first derivative of the microwave absorption signal with respect to an applied external magnetic field (H). The values A_1 and A_2 represent the coefficients of the symmetric and antisymmetric components of the FMR signal, respectively. Density-functional theory (DFT) calculations were performed by using Vienna *ab initio* simulation package (VASP).[31] These calculations estimated the DOS near E_F to assess the half-metallicity of the synthesized $Co_{44.3}Fe_{30.7}Ga_{13.9}Ge_{11.1}$ alloy composition. The results were compared with those of the stoichiometric $Co_{50}Fe_{25}Ga_{12.5}Ge_{12.5}$ alloy. Projector-augmented wave (PAW)[32] pseudopotentials were used to describe the interaction between valence electrons and ion cores. The exchange-correlation energy was evaluated within the generalized gradient approximation (GGA),[33] without considering the Coulomb interaction. The experimental lattice parameter ($a = 5.725$ Å), obtained from the XRD pattern, was used in all calculations. The Brillouin zone was

sampled using a $25 \times 25 \times 25$-point Monkhorst–Pack grid[34] to achieve sufficient k-point density. Chemical disorder between Co and Fe atoms, as well as Ga and Ge atoms in the $L2_1$-type structure, was modeled using the virtual crystal approximation (VCA).[35] It should be noted that previous studies[29,36,37] reported that VCA can correctly treat disorder only for elements that are neighbors in the periodic table. Therefore, VCA is appropriate for calculating the DOS for CFGG alloys, which exhibit disorder between Co and Fe, as well as Ga and Ge. The ideal CFGG $L2_1$ structure consists of two face-centered cubic sublattices with four atomic positions: two Co atoms at (0.25, 0.25, 0.25) and (0.75, 0.75, 0.75), one Fe atom at (0.5, 0.5, 0.5), and Ga and Ge atoms in a 50:50 ratio at (0, 0, 0). For the off-stoichiometric $Co_{44.3}Fe_{30.7}Ga_{13.9}Ge_{11.1}$ alloy, the atomic site occupancies were modified as follows: Co and Fe occupied the (0.25, 0.25, 0.25) and (0.75, 0.75, 0.75) sites in an 88.6%:11.4% ratio, Fe occupied the (0.5, 0.5, 0.5) site, and Ga and Ge occupied the (0, 0, 0) site in a 55.6%:44.4% ratio.

III. RESULTS AND DISCUSSION

A. First-principles calculations

First, we examined the DOS of CFGG with stoichiometric composition, along with the Co-deficient and Fe-rich off-stoichiometric composition used in the experiments. Figure 1(a) shows the calculated spin resolved total DOS for $Co_{50}Fe_{25}Ga_{12.5}Ge_{12.5}$ and $Co_{44.3}Fe_{30.7}Ga_{13.9}Ge_{11.1}$ compositions. In the off-stoichiometric composition, the DOS shifts horizontally and E_F is located closer to the middle of the gap, while the overall DOS shape is maintained. As a result, the spin polarization increased from 35% to 58%. We additionally calculated the sp-partial DOS, as shown in Fig. 1(b), because the electrons in the s and p bands are the primary contributors to electric conduction due to their high Fermi velocities. The estimated spin polarization of the sp-partial DOS is high, being 96% for stoichiometric CFGG and 94% for off-stoichiometric CFGG. Regarding the sum of majority and minority DOS at E_F, which is related to α, the same value of 1.166 states/eV was obtained for both stoichiometric and off-stoichiometric CFGG. However, Co–Fe disorder, which are expected to occur in stoichiometric CFGG, is known to give rise to an in-gap state in the minority band at E_F.[28,38] This in-gap state can increase α by increasing the sum of majority and minority DOS at E_F and disturbing the half-metallicity, from which we predict that off-stoichiometric CFGG can achieve lower α.

Figures 2(a) and 2(b) show the spin resolved band structures for $Co_{50}Fe_{25}Ga_{12.5}Ge_{12.5}$ and $Co_{44.3}Fe_{30.7}Ga_{13.9}Ge_{11.1}$ compositions, respectively. In both the compositions, a pseudo-gap is observed in the minority-spin channel around E_F, characterized by a substantial reduction in band dispersion and the absence of band crossings near E_F. In contrast, the majority-spin bands are metallic, with several bands crossing E_F, indicating metallic conduction in that channel. This behavior is consistent with that observed in the spin resolved total DOS. However, since the band structure does not exhibit a complete gap in the minority-spin channel, 100% half-metallicity is not realized. The presence of a pseudo-gap implies that the system lies near the half-metallic regime, but small perturbations such as atomic disorder can introduce states at E_F and significantly degrade the spin polarization. Notably, the off-stoichiometric composition exhibits a more pronounced separation of minority-spin bands near E_F, suggesting enhanced spin polarization and a system that more closely approaches half-metallicity, as predicted from the DOS analysis.

B. Structural characterization

Figures 3(a) and 3(b) show the out-of-plane ($\chi = 0°$) and ⟨111⟩-direction ($\chi = 54.7°$) 2θ-ω XRD patterns of the as-deposited and annealed samples, respectively. The presence of the 002 and 004 peaks in the out-of-plane XRD patterns indicate the epitaxial growth along the [001] direction in all the samples. The as-deposited and 400 °C-annealed samples exhibit a $B2$-type partially disordered structure as evidenced by the presence of 002 and the absence of 111 superlattice peaks. The samples annealed at $T_{an} = 500$ °C reveal a $L2_1$-ordered structure as evidenced by the appearance of 111 superlattice peak. Figure 3(c) shows the degree

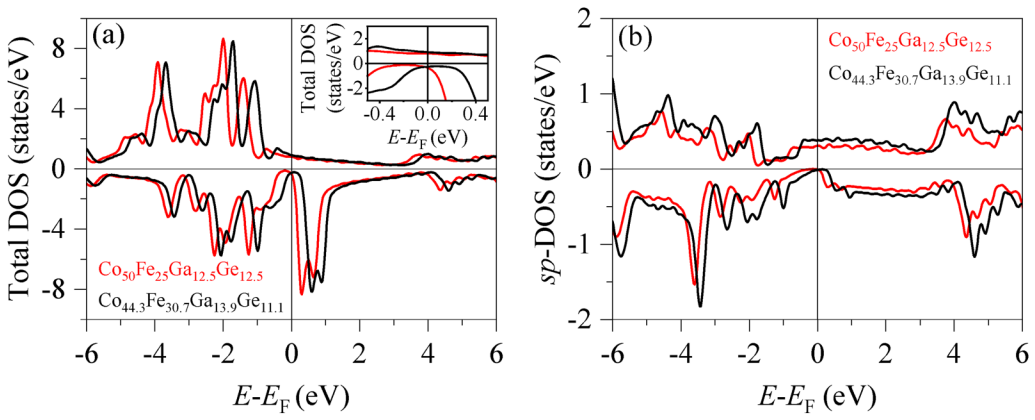

FIG. 1. (a) Spin resolved total DOS calculated for $Co_{50}Fe_{25}Ga_{12.5}Ge_{12.5}$ and $Co_{44.3}Fe_{30.7}Ga_{13.9}Ge_{11.1}$ composition. The inset in the figure provides an expanded view of DOS near E_F. (b) sp-DOS corresponding to $Co_{50}Fe_{25}Ga_{12.5}Ge_{12.5}$ and $Co_{44.3}Fe_{30.7}Ga_{13.9}Ge_{11.1}$ compositions.

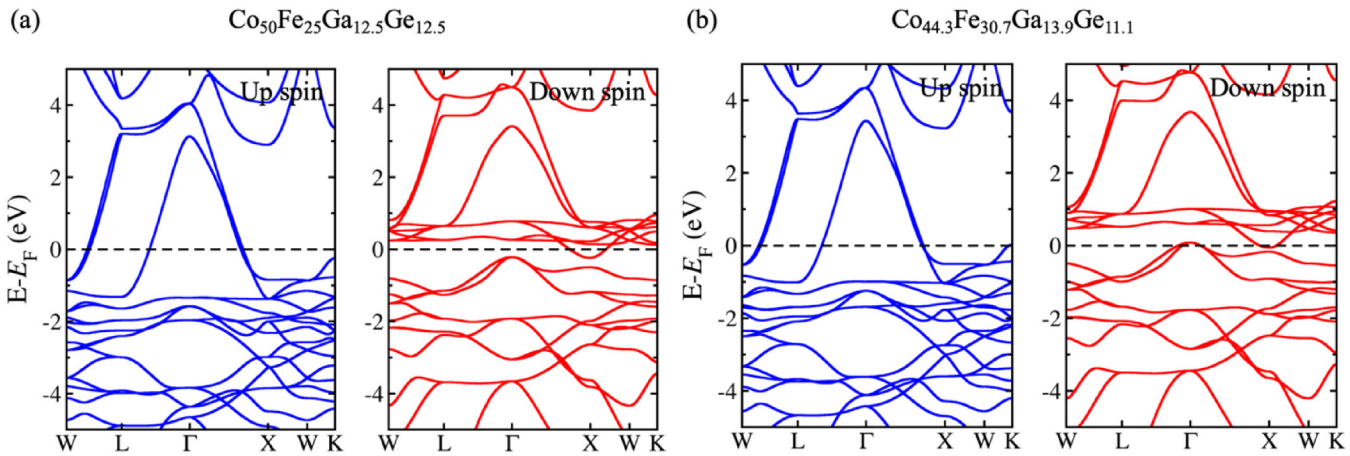

FIG. 2. Spin resolved band structures for (a) $Co_{50}Fe_{25}Ga_{12.5}Ge_{12.5}$ and (b) $Co_{44.3}Fe_{30.7}Ga_{13.9}Ge_{11.1}$ compositions. A pseudo-gap near E_F is evident in the minority-spin channel, consistent with the features observed in the DOS (see Fig. 1).

of $B2$ (S_{B2}) and $L2_1$ (S_{L2_1}) ordering expressed as[39]

$$S_{B2} = \sqrt{\frac{I_{002}^{obs}/I_{004}^{obs}}{I_{002}^{sim}/I_{004}^{sim}}}, \quad (2)$$

$$S_{L2_1} = \frac{2}{3 - S_{B2}} \sqrt{\frac{I_{111}^{obs}/I_{004}^{obs}}{I_{111}^{sim}/I_{004}^{sim}}}, \quad (3)$$

where I_{002}, I_{004}, and I_{111} indicate the integrated intensities of the 002, 004, and 111 XRD peaks, with the superscripts "obs" and "sim" correspond to the values observed in the experiments and simulation by VESTA software, respectively, for the Co-deficient and Fe-rich off-stoichiometric composition. Since the surface roughness is small (~0.7 nm), its influence on the experimentally observed XRD peak intensity is considered negligible in the analysis. During the simulation, the site occupations of each element follow the same configuration as the ones considered in the theoretical calculations. A high S_{B2} of 0.8 already obtained in the as-deposited sample increases slightly by increasing T_{an}. In contrast, S_{L2_1} which appears at $T_{an} = 500$ °C increases close to unity at $T_{an} = 600$ °C. Note that the presence of Co–Fe disorder is difficult to identify from standard XRD data because of the close atomic form factor of Co and Fe. The XRD using synchrotron radiated x rays enables the detection of disorder between the elements with close atomic form factor through the change in anomalous dispersion term of atomic form factor at the absorption edges of the constituent elements. This method is called anomalous XRD. A previous study of anomalous XRD on CFGG reported that substantial Co–Fe disorder existed in the as-deposited sample and the amount of disorder decreased with increasing T_{an} up to 500 °C.[28] Based on this report, we speculate that a similar type of Co–Fe disorder exists in our sample annealed at $T_{an} \leq 400$ °C. Moreover, it can be inferred from

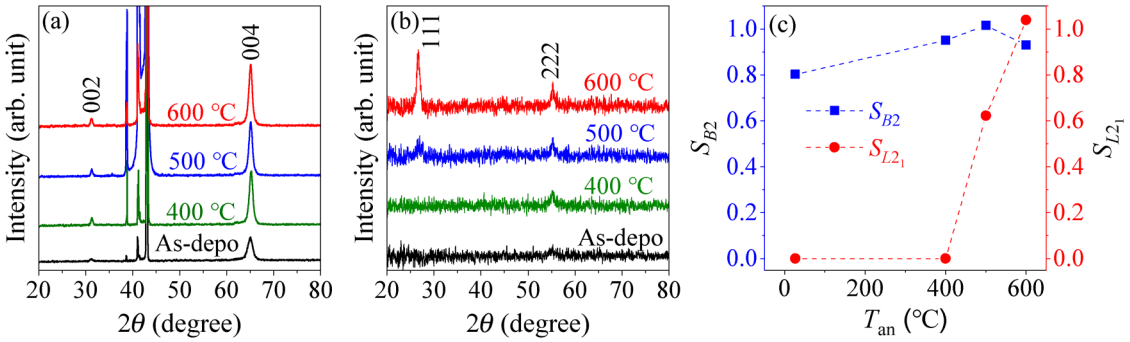

FIG. 3. XRD patterns of 2θ-ω scans of as-deposited and annealed samples at tilt angles (a) $\chi = 0°$ and (b) $\chi = 54.7°$. (c) Dependence of S_{B2} and S_{L2_1} parameters of the sample on annealing temperature T_{an}.

Chen *et al.*[29] that the $Co_{44.3}Fe_{30.7}Ga_{13.9}Ge_{11.1}$ thin films annealed at $T_{an} \geq 500$ °C can be presumed to be free of Co–Fe disorder.

C. Magnetoresistance

To investigate the variation in half-metallicity with improvement in atomic order achieved by annealing, the AMR ratio was measured at measurement temperatures (T) from 50 to 300 K, with 50 K intervals. Figure 4(a) shows the angular variation in AMR ratio measured at $T = 50$ K for the as-deposited and annealed samples. All the samples show negative AMR and the amplitude of the negative AMR ratio increases with increasing T_{an}. Figure 4(b) shows the temperature dependence of $\Delta\rho_{AMR}$ normalized by the value at $T = 50$ K. Here, $\Delta\rho_{AMR}$ is defined as the difference in the electrical resistivity when the magnetic field and current directions are parallel and perpendicular.[29] The as-deposited sample shows the largest reduction in the normalized $\Delta\rho_{AMR}$ with increasing T. Such behavior is largely decreased in the annealed samples, and $\Delta\rho_{AMR}$ became almost constant at $T_{an} = 500$ °C and 600 °C. The negative AMR ratio is considered a signature of half-metallicity,[40–42] as discussed below, though it is not conclusive evidence.[38]

According to the two-current model for the evaluation of $\Delta\rho_{AMR}$ in half-metallic ferromagnetic materials, only $s_\uparrow \rightarrow d_\downarrow$ and $s_\uparrow \rightarrow d_\uparrow$ types of scattering processes are taken into consideration (subscripts $\uparrow$ and $\downarrow$ refer to up and down spin, respectively). Hence, $\Delta\rho_{AMR}$ can be expressed as[38]

$$\Delta\rho_{AMR} \approx \gamma(\rho_{s,\uparrow\rightarrow d,\downarrow} - \rho_{s,\uparrow\rightarrow d,\uparrow}) \propto D_\uparrow^{(d)}(E_F)\left[1 - \frac{D_\downarrow^{(d)}(E_F)}{D_\uparrow^{(d)}(E_F)}\right]. \quad (4)$$

Here, $D_\uparrow^{(d)}(E_F)$ and $D_\downarrow^{(d)}(E_F)$ represent the d-orbital DOS at E_F for up and down spins, respectively. The temperature dependence of $\Delta\rho_{AMR}$ originated primarily from the $D_\downarrow^{(d)}(E_F)$ due to the thermally excited electrons governed by the Fermi–Dirac distribution function. In the case of $L2_1$-ordered off-stoichiometric CFGG, $D_\downarrow^{(d)}(E_F)$ is nearly zero with E_F located near the middle of the gap, as seen in the calculated d-orbital DOS in Fig. 4(c). This electronic structure indicates that near-zero $D_\downarrow^{(d)}(E_F)$ is robust against temperature increase. Therefore, $\Delta\rho_{AMR}$ is expected to be constant, as observed in the $L2_1$-ordered sample for $T_{an} \geq 500$ °C. On the other hand, a substantial $D_\downarrow^{(d)}(E_F)$ in the gap due to the Co–Fe disorder is expected in the as-deposited and 400 °C-annealed samples.[28,38] In this scenario, Eq. (4) does not hold because of the existence of other types of s-d scattering processes, such as $s_\downarrow \rightarrow d_\downarrow$ and $s_\downarrow \rightarrow d_\uparrow$ along with $s_\uparrow \rightarrow d_\downarrow$ and $s_\uparrow \rightarrow d_\uparrow$, which explain the large temperature dependence in $\Delta\rho_{AMR}$. The above analysis qualitatively confirms an enhancement in half-metallicity with an improvement in the atomic order in the samples by increasing T_{an}.

Further, the enhancement in half-metallicity with the improved atomic order was analyzed by OMR measurements. Figures 5(a)–5(d) show the variation of OMR ratio calculated by $\Delta\rho_{OMR}/\rho_0$ as a function of external magnetic field for the as-deposited and 400, 500, and 600 °C annealed samples, respectively. Here, $\Delta\rho_{OMR} = \rho_H - \rho_0$ with ρ_H and ρ_0 representing the electrical resistivity in the presence and absence of a magnetic field, respectively. In all the samples, the OMR ratio exhibits a negative slope with respect to the magnetic field, and the slope increases with decreasing measurement temperature. In the comparison among the samples with different T_{an}, the slopes show an increasing trend with increasing T_{an}, as discussed below.

In general, the electrical resistivity of a ferromagnetic material can be decomposed to three components, *viz.*, $\rho(T) = \rho_R + \rho_P(T) + \rho_M(T)$,[43,44] where ρ_R, $\rho_P(T)$, and $\rho_M(T)$ are resistivity due to temperature independent electron-defect scattering, temperature-dependent scattering of electrons by phonons, and temperature-dependent scattering of electrons by magnons, respectively. At room temperature, $\rho_M(T)$ is sensitive to the magnetic field and decreases with increasing magnetic field due to the suppression of electron–magnon scattering, which leads to negative magnetoresistance.[45]

In half-metallic ferromagnets, the absence of minority DOS at E_F results in an exponential suppression of $\rho_M(T)$, i.e., $\rho_M(T)e^{-\Delta/k_B T}$,[43,44] where Δ represents the lowest excitation energy for spin-flip process of majority charge carriers, as depicted in Fig. 5(e), and k_B is the Boltzmann constant. At low temperature, this additional factor suppresses $\rho_M(T)$. Additionally, low temperature reduces lattice vibration, diminishing $\rho_P(T)$. In this scenario, ρ_R becomes dominant, where the Lorentz force causes electrons to

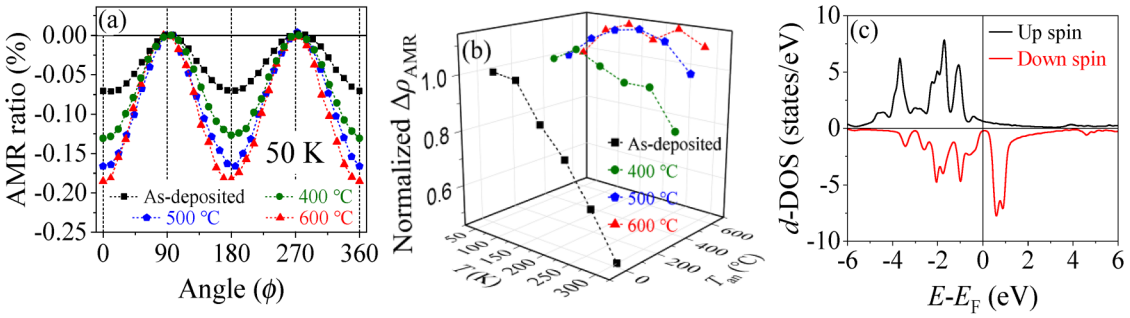

FIG. 4. (a) Angular dependence of AMR ratio of the samples recorded at 50 K. (b) Measurement temperature dependence of normalized $\Delta\rho_{AMR}$ for various samples with different T_{an}. (c) d-orbital DOS of off-stoichiometric CFGG with $L2_1$ ordered structure.

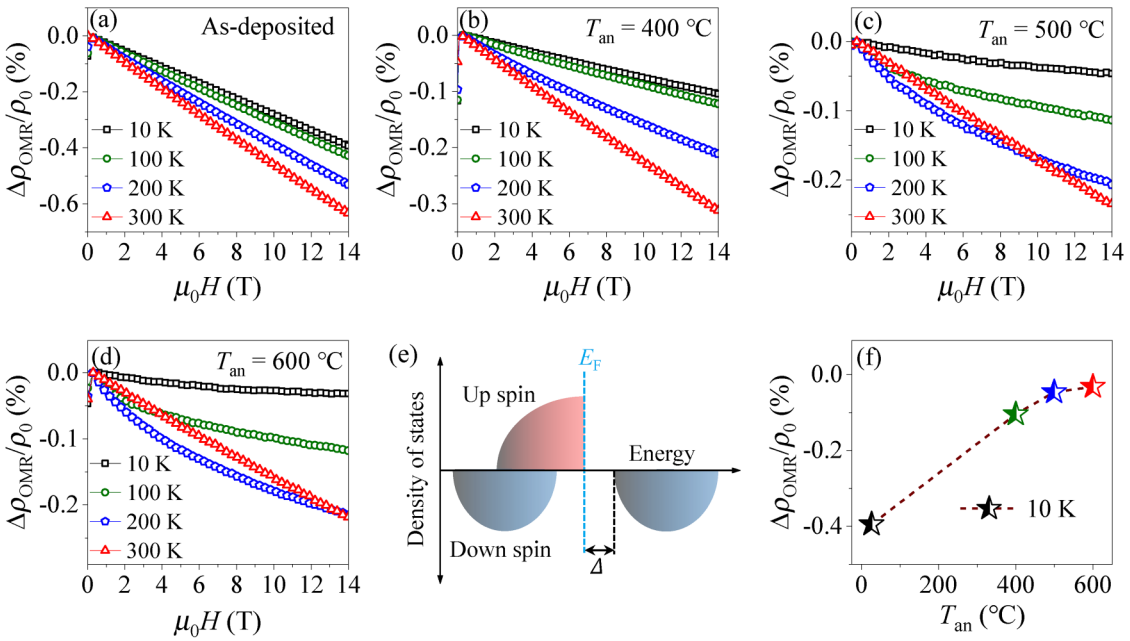

FIG. 5. Variation of OMR ratio with applied magnetic field measured at 10, 100, 200, and 300 K for (a) as-deposited, (b) T_{an} = 400 °C, (c) T_{an} = 500 °C, and (d) T_{an} = 600 °C samples. (e) Schematic of DOS *vs* energy plot of a half-metal. (f) T_{an} dependence of OMR ratio measured with a field of 14 T at 10 K.

travel longer paths in a magnetic field, leading to an increase in $\rho(T)$.[46] Therefore, the OMR ratio increases with decreasing temperature. The OMR ratio at 10 K increases with increasing T_{an}, as shown in Fig. 5(f), and this increase is attributed to the increase in Δ and resultant higher suppression of $\rho_M(T)$. As Δ is directly linked to half-metallicity, the increase in the OMR ratio signifies the improved half-metallicity of the material with T_{an}.

Goto *et al.*[28] have shown an improvement in spin polarization of CFGG as the *B*2 disorder changes to $L2_1$ order. Based on this report, the enhancement in the $L2_1$ order by increasing T_{an} from 400 to 600 °C explains the improved half-metallicity. However, the improvement in the half-metallicity between the as-deposited and 400 °C-annealed samples cannot be explained on this basis because both samples do not exhibit $L2_1$ ordering, suggesting the effect of the Co–Fe disorder. As reported in the anomalous XRD study, the Co–Fe disorder gives rise to the minority DOS at E_F, deteriorating the half-metallicity.[28,38] Since the amount of Co–Fe disorder decreases continuously with increasing T_{an} and ultimately vanishes at $T_{an} \geq 500$ °C, half-metallicity of the 400 °C-annealed samples improves from that of the as-deposited sample.

D. Magnetodynamic properties

To investigate the relation between α_{int} and half-metallicity, FMR measurements at room temperature were performed. Figure 6(a) shows the typical FMR spectrum with fitting by Eq. (1) to evaluate the resonance field ($\mu_0 H_r$) and linewidth ($\mu_0 \Delta H$).[30] The obtained $\mu_0 H_r$ with the corresponding resonance frequency (f) was plotted, as shown in Fig. 6(b), to evaluate the gyromagnetic ratio (γ) by fitting the data to the Kittel equation.[47] The estimated γ was used to evaluate the total Gilbert damping constant (α_{total}) by fitting the $\mu_0 \Delta H$ vs f plot [shown in Fig. 6(c)] with the relation,[48]

$$\mu_0 \Delta H = \frac{4\pi \alpha_{total}}{\gamma} f + \mu_0 \Delta H_0, \tag{5}$$

where $\mu_0 \Delta H_0$ is the intrinsic linewidth. The experimentally obtained α_{total} from Eq. (5) is $\sim(7.3 \pm 0.3) \times 10^{-4}$, which contains both intrinsic (α_{int}) and extrinsic (α_{ext}) components. α_{ext} consists of contributions from two-magnon scattering (α_{TMS}), spin pumping (α_{sp}), radiative damping (α_{rad}), and eddy current (α_{eddy}).[49] Here, α_{TMS} is neglected because of the high frequencies used in the FMR measurements.[10] Spin pumping is also neglected by considering the low spin–orbit coupling of the Al capping layer and its thickness is less than the spin diffusion length. The third contribution α_{rad}, arising from the interaction between magnetization precession and the co-planar waveguide, is estimated to be $\sim 3.7 \times 10^{-4}$, according to the report by Schoen *et al.*[50] The last contribution arises from the eddy current induced by alternating magnetic field is estimated to be $\sim 1 \times 10^{-5}$.[49] By subtracting all the extrinsic contributions from α_{total}, α_{int} was determined. Figure 6(d) shows the T_{an} dependence of α_{total} and α_{int}. The α_{int} value decreases with increasing T_{an} up to 500 °C and decreases slightly upon further increasing T_{an} to 600 °C, reaching the very low value of $(3.5 \pm 0.3) \times 10^{-4}$. This decreasing trend in α_{int} coincides with that of the enhanced half-metallicity revealed in the AMR and OMR measurements, supporting their relation.

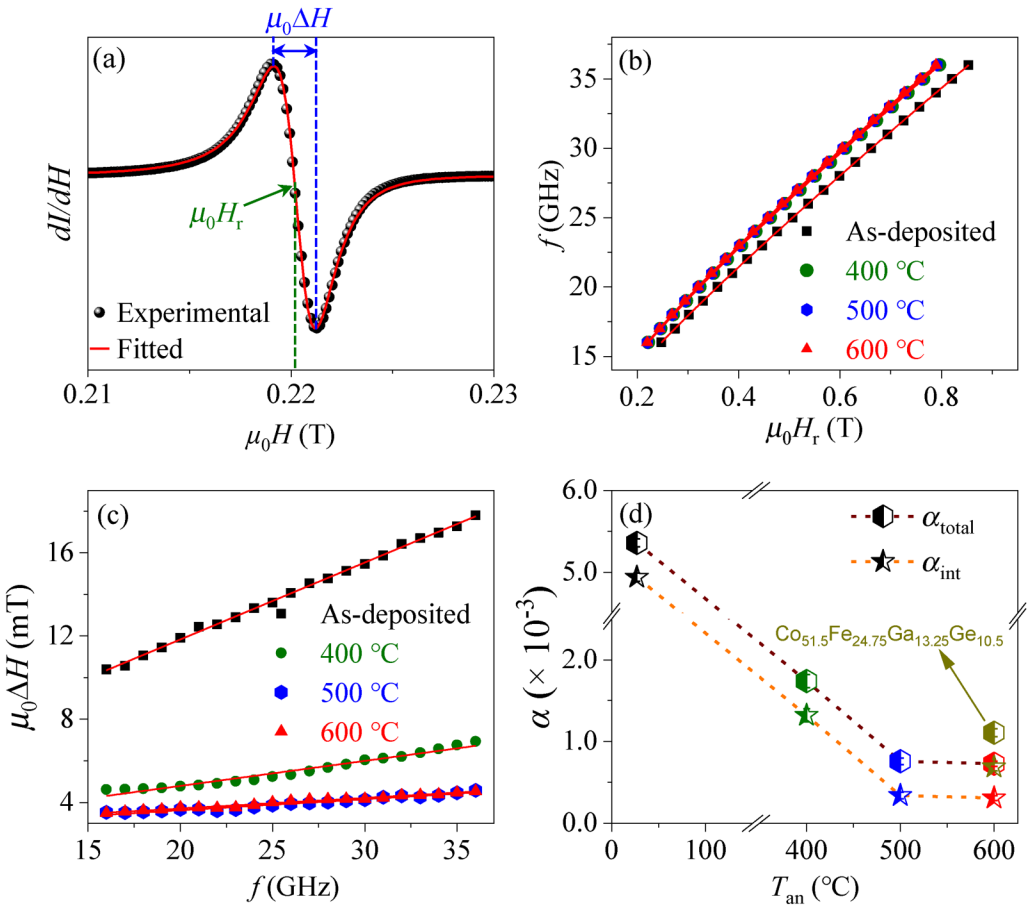

FIG. 6. (a) Typical FMR spectrum of the off-stoichiometric CFGG thin film. (b) Variation of $\mu_0 H_r$ with resonance frequency along with fit to the Kittel equation. (c) Variation of $\mu_0\Delta H$ as a function of resonance frequency of the samples along with fit to Eq. (5). (d) Variation of α_{total} and α_{int} with T_{an} for $Co_{44.3}Fe_{30.7}Ga_{13.9}Ge_{11.1}$ along with α_{total} and α_{int} values for $Co_{51.5}Fe_{24.75}Ga_{13.25}Ge_{10.5}$ annealed at 600 °C.

Since α_{int} is directly proportional to the sum of majority and minority DOS at E_F, its reduction by the enhanced half-metallicity leads to a reduction in α_{int}. In comparison, non-conducting Yttrium Iron Garnet exhibits much lower α_{total} of $(8.58 \pm 0.21) \times 10^{-5}$.[51] However, achieving low α_{total} in conducting materials is essential for charge-based spintronic devices. Among conducting materials, $Co_{25}Fe_{25}$ showed α_{int} of 5.0×10^{-4} and α_{total} ranging from $\sim 1.4 \times 10^{-3}$ to 2.1×10^{-3},[2,52,53] while NiFe and CoFeB exhibited α_{total} of $\sim 4.6 \times 10^{-3}$ to 5.5×10^{-3} and 4.2×10^{-3}, respectively.[54,55] These reported values are higher than the obtained α in this study for $Co_{44.3}Fe_{30.7}Ga_{13.9}Ge_{11.1}$. Furthermore, we fabricated $Co_{51.5}Fe_{24.75}Ga_{13.25}Ge_{10.5}$ films with a composition close to the stoichiometric CFGG. The α_{int} of this CFGG film annealed at $T_{an} = 600$ °C was found to be $(6.9 \pm 0.5) \times 10^{-4}$, as shown in Fig. 6(d), which is higher than that of the $Co_{44.3}Fe_{30.7}Ga_{13.9}Ge_{11.1}$ film ($(3.5 \pm 0.3) \times 10^{-4}$) annealed at the same T_{an}, highlighting its advantage for obtaining low α.

IV. CONCLUSIONS

In summary, we studied α in off-stoichiometric Co-deficient and Fe-rich CFGG Heusler alloy thin films annealed at different T_{an} using FMR measurements and demonstrated very low α. We also investigated the relation of α with atomic ordering and half-metallicity. The CFGG thin films were prepared by magnetron sputtering and annealed *in situ* at $T_{an} = 400$, 500, and 600 °C to improve the atomic ordering. Structural analysis confirmed the presence of a *B*2-type disordered structure in the as-deposited sample. $L2_1$ ordering appeared at $T_{an} = 500$ °C and improved as T_{an} was increased to 600 °C. The effect of atomic ordering on the half-metallicity was explored through AMR and OMR measurements, which indicated an improvement in half-metallicity with increasing T_{an} due to the improved atomic ordering. The enhancement in half-metallicity is reflected in the low value of α_{int}. The α_{int} value decreased significantly with increasing T_{an} up to 500 °C, and further increasing T_{an} to 600 °C slightly decreased α_{int}, achieving a

remarkably low α_{int} of $(3.5 \pm 0.3) \times 10^{-4}$. These results demonstrated that off-stoichiometric CFGG is a promising material to reduce the critical current density and pave the way for the realization of highly energy-efficient spintronic devices.

ACKNOWLEDGMENTS

The authors thank S. Kuramochi and N. Kojima, NIMS, for their support in the film preparation and characterizations. This work was supported by the Advanced Storage Research Consortium (ASRC), JST CREST under Grant No. JPMJCR21O1, and the MEXT Initiative to Establish Next-generation Novel Integrated Circuits Centers (X-NICS) under Grant No. JPJ011438.

AUTHOR DECLARATIONS

Conflict of Interest

The authors have no conflicts to disclose.

Author Contributions

Madhav M. Bhat: Formal analysis (equal); Investigation (lead); Visualization (lead); Writing – original draft (lead). **K. Simalaotao:** Formal analysis (lead); Writing – review & editing (equal). **H. Suto:** Conceptualization (lead); Investigation (equal); Supervision (equal); Writing – review & editing (lead). **A. Perumal:** Conceptualization (equal); Supervision (equal); Writing – review & editing (equal). **A. Srinivasan:** Conceptualization (equal); Supervision (equal); Writing – review & editing (equal). **Y. Sakuraba:** Conceptualization (equal); Supervision (lead); Writing – review & editing (equal).

DATA AVAILABILITY

The data that support the findings of this study are available from the corresponding author upon reasonable request.

REFERENCES

[1]Y. Fan, J. Wang, A. Chen, K. Yu, M. Zhu, Y. Han, S. Zhang, X. Lin, H. Zhou, X. Zhang, and Q. Lin, "Thickness-dependent Gilbert damping and soft magnetism in metal/Co-Fe-B/metal sandwich structure," Nanomaterials **14**, 596 (2024).
[2]M. A. W. Schoen, D. Thonig, M. L. Schneider, T. J. Silva, H. T. Nembach, O. Eriksson, O. Karis, and J. M. Shaw, "Ultra-low magnetic damping of a metallic ferromagnet," Nat. Phys. **12**, 839–842 (2016).
[3]M. Tokaç, S. A. Bunyaev, G. N. Kakazei, D. S. Schmool, D. Atkinson, and A. T. Hindmarch, "Interfacial structure dependent spin mixing conductance in cobalt thin films," Phys. Rev. Lett. **115**, 056601 (2015).
[4]P. Kuświk, H. Głowiński, E. Coy, J. Dubowik, and F. Stobiecki, "Perpendicularly magnetized $Co_{20}Fe_{60}B_{20}$ layer sandwiched between Au with low Gilbert damping," J. Phys.: Condens. Matter **29**, 435803 (2017).
[5]C. Swindells, H. Głowiński, Y. Choi, D. Haskel, P. P. Michałowski, T. Hase, P. Kuświk, and D. Atkinson, "Proximity-induced magnetism and the enhancement of damping in ferromagnetic/heavy metal systems," Appl. Phys. Lett. **119**, 152401 (2021).
[6]C. Swindells, H. Głowiński, Y. Choi, D. Haskel, P. P. Michałowski, T. Hase, F. Stobiecki, P. Kuświk, and D. Atkinson, "Magnetic damping in ferromagnetic/heavy-metal systems: The role of interfaces and the relation to proximity-induced magnetism," Phys. Rev. B **105**, 094433 (2022).
[7]S. Azzawi, A. Umerski, L. C. Sampaio, S. A. Bunyaev, G. N. Kakazei, and D. Atkinson, "Synthetic route to low damping in ferromagnetic thin-films," APL Mater. **11**(8), 081108 (2023).
[8]Z. Jiang, A. Hoffmann, and A. Schleife, "Influence of temperature, doping, and amorphization on the electronic structure and magnetic damping of iron," Phys. Rev. B **109**(23), 235147 (2024).
[9]T. Kubota, S. Tsunegi, M. Oogane, S. Mizukami, T. Miyazaki, H. Naganuma, and Y. Ando, "Half-metallicity and Gilbert damping constant in $Co_2Fe_xMn_{1-x}Si$ Heusler alloys depending on the film composition," Appl. Phys. Lett. **94**, 122504 (2009).
[10]S. Mizukami, D. Watanabe, M. Oogane, Y. Ando, Y. Miura, M. Shirai, and T. Miyazaki, "Low damping constant for Co_2FeAl Heusler alloy films and its correlation with density of states," J. Appl. Phys. **105**, 07D–306 (2009).
[11]J. M. Shaw, E. K. Delczeg-Czirjak, E. R. J. Edwards, Y. Kvashnin, D. Thonig, M. A. W. Schoen, M. Pufall, M. L. Schneider, T. J. Silva, O. Karis, K. P. Rice, O. Eriksson, and H. T. Nembach, "Magnetic damping in sputter-deposited Co_2MnGe Heusler compounds with *A*2, *B*2, and $L2_1$ orders: Experiment and theory," Phys. Rev. B **97**, 094420 (2018).
[12]R. Mahat, S. KC, U. Karki, J. Y. Law, V. Franco, I. Galanakis, A. Gupta, and P. LeClair, "Possible half-metallic behavior of $Co_{2-x}Cr_xFeGe$ Heusler alloys: Theory and experiment," Phys. Rev. B **104**(1), 014430 (2021).
[13]R. Mahat, U. Karki, S. Kc, J. Y. Law, V. Franco, I. Galanakis, A. Gupta, and P. Leclair, "Effect of mixing the low-valence transition metal atoms Y = Co, Fe, Mn, Cr, V, Ti, or Sc on the properties of quaternary Heusler compounds $Co_{2-x}Y_xFeSi$ $(0 \le x \le 1)$," Phys. Rev. Mater. **6**(6), 064413 (2022).
[14]S. Andrieu, A. Neggache, T. Hauet, T. Devolder, A. Hallal, M. Chshiev, A. M. Bataille, P. Le Fèvre, and F. Bertran, "Direct evidence for minority spin gap in the Co_2MnSi Heusler compound," Phys. Rev. B **93**, 094417 (2016).
[15]C. Guillemard, S. Petit-Watelot, L. Pasquier, D. Pierre, J. Ghanbaja, J. C. Rojas-Sánchez, A. Bataille, J. Rault, P. Le Fèvre, F. Bertran, and S. Andrieu, "Ultralow magnetic damping in Co_2Mn-based Heusler compounds: Promising materials for spintronics," Phys. Rev. Appl. **11**, 064009 (2019).
[16]V. Barwal, H. Suto, R. Toyama, K. Simalaotao, T. Sasaki, Y. Miura, and Y. Sakuraba, "Large magnetoresistance and high spin-transfer torque efficiency of $Co_2Mn_xFe_{1-x}Ge$ $(0 \le x \le 1)$ Heusler alloy thin films obtained by high-throughput compositional optimization using combinatorially sputtered composition-gradient film," APL Mater. **12**, 111114 (2024).
[17]Y. K. Takahashi, A. Srinivasan, B. Varaprasad, A. Rajanikanth, N. Hase, T. M. Nakatani, S. Kasai, T. Furubayashi, and K. Hono, "Large magnetoresistance in current-perpendicular-to-plane pseudospin valve using a $Co_2Fe(Ge_{0.5}Ga_{0.5})$ Heusler alloy," Appl. Phys. Lett. **98**, 152501 (2011).
[18]S. Li, Y. K. Takahashi, T. Furubayashi, and K. Hono, "Enhancement of giant magnetoresistance by $L2_1$ ordering in $Co_2Fe(Ge_{0.5}Ga_{0.5})$ Heusler alloy current-perpendicular-to-plane pseudo spin valves," Appl. Phys. Lett. **103**, 042405 (2013).
[19]J. W. Jung, Y. Sakuraba, T. T. Sasaki, Y. Miura, and K. Hono, "Enhancement of magnetoresistance by inserting thin NiAl layers at the interfaces in $Co_2FeGa_{0.5}Ge_{0.5}$/Ag/$Co_2FeGa_{0.5}Ge_{0.5}$ current-perpendicular-to-plane pseudo spin valves," Appl. Phys. Lett. **108**, 102408 (2016).
[20]B. S. D. C. S. Varaprasad, A. Srinivasan, Y. K. Takahashi, M. Hayashi, A. Rajanikanth, and K. Hono, "Spin polarization and Gilbert damping of $Co_2Fe(Ga_xGe_{1-x})$ Heusler alloys," Acta Mater. **60**, 6257–6265 (2012).
[21]B. S. D. C. S. Varaprasad, A. Rajanikanth, Y. K. Takahashi, and K. Hono, "Enhanced spin polarization of Co_2MnGe Heusler alloy by substitution of Ga for Ge," Appl. Phys. Express **3**, 023002 (2010).
[22]Y. Sakuraba, K. Izumi, T. Iwase, S. Bosu, K. Saito, K. Takanashi, Y. Miura, K. Futatsukawa, K. Abe, and M. Shirai, "Mechanism of large magnetoresistance in Co_2MnSi/Ag/Co_2MnSi devices with current perpendicular to the plane," Phys. Rev. B **82**, 094444 (2010).
[23]Y. Sakuraba, M. Ueda, Y. Miura, K. Sato, S. Bosu, K. Saito, M. Shirai, T. J. Konno, and K. Takanashi, "Extensive study of giant magnetoresistance properties in half-metallic $Co_2(Fe,Mn)Si$-based devices," Appl. Phys. Lett. **101**, 252408 (2012).

[24]Y. K. Takahashi, N. Hase, M. Kodzuka, A. Itoh, T. Koganezawa, T. Furubayashi, S. Li, B. Varaprasad, T. Ohkubo, and K. Hono, "Structure and magnetoresistance of current-perpendicular-to-plane pseudo spin valves using $Co_2Mn(Ga_{0.25}Ge_{0.75})$ Heusler alloy," J. Appl. Phys. **113**, 223901 (2013).
[25]H. Narisawa, T. Kubota, and K. Takanashi, "Erratum: Current perpendicular to film plane type giant magnetoresistance effect using a Ag–Mg spacer and $Co_2Fe_{0.4}Mn_{0.6}Si$ Heusler alloy electrodes," Appl. Phys. Express **8**, 119201 (2015).
[26]Y. Sakuraba, K. Izumi, S. Bosu, K. Saito, and K. Takanashi, "Temperature dependence of spin-dependent transport properties of Co_2MnSi-based current-perpendicular to-plane magnetoresistive devices," J. Phys. D: Appl. Phys. **44**, 064009 (2011).
[27]M. Inoue, K. Inubushi, D. Mouri, T. Tanimoto, K. Nakada, K. Kondo, M. Yamamoto, and T. Uemura, "Origin of biquadratic interlayer exchange coupling in Co_2MnSi-based current-perpendicular-to-plane pseudo spin valves," Appl. Phys. Lett. **114**, 062401 (2019).
[28]K. Goto, L. S. R. Kumara, Y. Sakuraba, Y. Miura, I. Kurniawan, A. Yasui, H. Tajiri, Y. Fujita, Z. Chen, and K. Hono, "Effects of the atomic order on the half-metallic electronic structure in the $Co_2Fe(Ga_{0.5}Ge_{0.5})$ Heusler alloy thin film," Phys. Rev. Mater. **4**, 114406 (2020).
[29]Z. Chen, Y. Sakuraba, Y. Miura, Z. Li, T. Sasaki, H. Suto, V. K. Kushwaha, T. Nakatani, S. Mitani, and K. Hono, "Phase stability and half-metallic character of off-stoichiometric $Co_2FeGa_{0.5}Ge_{0.5}$ Heusler alloys," J. Appl. Phys. **132**, 183902 (2022).
[30]A. Kumar, R. Gupta, S. Husain, N. Behera, S. Hait, S. Chaudhary, R. Brucas, and P. Svedlindh, "Spin pumping and spin torques in interfacially tailored Co_2FeAl/β-Ta layers," Phys. Rev. B **100**, 214433 (2019).
[31]G. Kresse and J. Hafner, "*Ab initio* molecular dynamics for liquid metals," Phys. Rev. B **47**, 558–561 (1993).
[32]G. Kresse and D. Joubert, "From ultrasoft pseudopotentials to the projector augmented-wave method," Phys. Rev. B **59**, 1758–1775 (1999).
[33]J. P. Perdew, K. Burke, and M. Ernzerhof, "Generalized gradient approximation made simple," Phys. Rev. Lett. **77**, 3865–3868 (1996).
[34]H. J. Monkhorst and J. D. Pack, "Special points for Brillonin-zone integrations," Phys. Rev. B **13**, 5188–5192 (1976).
[35]C. Eckhardt, K. Hummer, and G. Kresse, "Indirect-to-direct gap transition in strained and unstrained Sn_xGe_{1-x} alloys," Phys. Rev. B **89**, 165201 (2014).
[36]C. J. Yu and H. Emmerich, "An efficient virtual crystal approximation that can be used to treat heterovalent atoms, applied to $(1-x)BiScO_{3-x}PbTiO_3$," J. Phys.: Condens. Matter **19**, 306203 (2007).
[37]U. G. Jong, C. J. Yu, Y. S. Kim, Y. H. Kye, and C. H. Kim, "First-principles study on the material properties of the inorganic perovskite $Rb_{1-x}Cs_xPbI_3$ for solar cell applications," Phys. Rev. B **98**, 125116 (2018).
[38]V. K. Kushwaha, S. Kokado, S. Kasai, Y. Miura, T. Nakatani, R. Kumara, H. Tajiri, T. Furubayashi, K. Hono, and Y. Sakuraba, "Prediction of half-metallic gap formation and Fermi level position in Co-based Heusler alloy epitaxial thin films through anisotropic magnetoresistance effect," Phys. Rev. Mater. **6**, 064411 (2022).
[39]R. Modak, K. Goto, S. Ueda, Y. Miura, K. I. Uchida, and Y. Sakuraba, "Combinatorial tuning of electronic structure and thermoelectric properties in $Co_2MnAl_{1-x}Si_x$ Weyl semimetals," APL Mater. **9**, 031105 (2021).
[40]F. J. Yang, Y. Sakuraba, S. Kokado, Y. Kota, A. Sakuma, and K. Takanashi, "Anisotropic magnetoresistance in $Co_2(Fe,Mn)Si$ Heusler epitaxial films: A fingerprint of half-metallicity," Phys. Rev. B **86**, 020409(R) (2012).
[41]Y. Sakuraba, S. Kokado, Y. Hirayama, T. Furubayashi, H. Sukegawa, S. Li, Y. K. Takahashi, and K. Hono, "Quantitative analysis of anisotropic magnetoresistance in Co_2MnZ and Co_2FeZ epitaxial thin films: A facile way to investigate spin-polarization in half-metallic Heusler compounds," Appl. Phys. Lett. **104**, 172407 (2014).
[42]J. Chen, Y. Sakuraba, K. Masuda, Y. Miura, S. Li, S. Kasai, T. Furubayashi, and K. Hono, "Enhancement of $L2_1$ order and spin-polarization in Co_2FeSi thin film by substitution of Fe with Ti," Appl. Phys. Lett. **110**, 242401 (2017).
[43]D. Bombor, C. G. F. Blum, O. Volkonskiy, S. Rodan, S. Wurmehl, C. Hess, and B. Büchner, "Half-metallic ferromagnetism with unexpectedly small spin splitting in the Heusler compound Co_2FeSi," Phys. Rev. Lett. **110**, 066601 (2013).
[44]S. Chatterjee, S. Samanta, B. Ghosh, and K. Mandal, "Half-metallic ferromagnetism and intrinsic anomalous Hall effect in the topological Heusler compound Co_2MnGe," Phys. Rev. B **108**, 205108 (2023).
[45]A. Patra, K. P. Maity, and V. Prasad, "Influence of orbital two-channel Kondo effect on anomalous Hall effect in ferrimagnetic composites of $LaNiO_3$ and $CoFe_2O_4$," J. Phys.: Condens. Matter **31**, 255702 (2019).
[46]I. Bakonyi, F. D. Czeschka, L. F. Kiss, V. A. Isnaini, A. T. Krupp, K. Palotás, S. Zsurzsa, and L. Péter, "High-field magnetoresistance of microcrystalline and nanocrystalline Ni metal at 3 K and 300 K," Eur. Phys. J. Plus **137**, 871 (2022).
[47]S. S. Kalarickal, P. Krivosik, M. Wu, C. E. Patton, M. L. Schneider, P. Kabos, T. J. Silva, and J. P. Nibarger, "Ferromagnetic resonance linewidth in metallic thin films: Comparison of measurement methods," J. Appl. Phys. **99**, 093909 (2006).
[48]A. Kumar, F. Pan, S. Husain, S. Akansel, R. Brucas, L. Bergqvist, S. Chaudhary, and P. Svedlindh, "Temperature-dependent Gilbert damping of Co_2FeAl thin films with different degree of atomic order," Phys. Rev. B **96**, 224425 (2017).
[49]S. Hait, S. Husain, V. Barwal, N. K. Gupta, L. Pandey, P. Svedlindh, and S. Chaudhary, "Comparison of high temperature growth versus post-deposition *in situ* annealing in attaining very low Gilbert damping in sputtered Co_2FeAl Heusler alloy films," J. Magn. Magn. Mater. **519**, 167509 (2021).
[50]M. A. W. Schoen, J. M. Shaw, H. T. Nembach, M. Weiler, and T. J. Silva, "Radiative damping in waveguide-based ferromagnetic resonance measured via analysis of perpendicular standing spin waves in sputtered permalloy films," Phys. Rev. B **92**, 184417 (2015).
[51]H. Chang, P. Li, W. Zhang, T. Liu, A. Hoffmann, L. Deng, and M. Wu, "Nanometer-thick yttrium iron Garnet films with extremely low damping," IEEE Magn. Lett. **5**, 6700104 (2014).
[52]A. J. Lee, J. T. Brangham, Y. Cheng, S. P. White, W. T. Ruane, B. D. Esser, D. W. McComb, P. C. Hammel, and F. Yang, "Metallic ferromagnetic films with magnetic damping under 1.4×10^{-3}," Nat. Commun. **8**, 234 (2017).
[53]E. R. J. Edwards, H. T. Nembach, and J. M. Shaw, "$Co_{25}Fe_{75}$ thin films with ultralow total damping of ferromagnetic resonance," Phys. Rev. Appl. **11**, 054036 (2019).
[54]A. Conca, J. Greser, T. Sebastian, S. Klingler, B. Obry, B. Leven, and B. Hillebrands, "Low spin-wave damping in amorphous $Co_{40}Fe_{40}B_{20}$ thin films," J. Appl. Phys. **113**, 213909 (2013).
[55]K. F. Dong, Y. Y. Jiao, Z. Y. Yuan, C. Sun, K. H. He, F. Jin, W. Q. Mo, and J. L. Song, "Low magnetic damping of epitaxial NiFe (100) thin films grown on different substrate," J. Magn. Magn. Mater. **523**, 167615 (2021).